



## Formation of nanoclusters with varying Pb/Se concentration and distribution after sequential Pb<sup>+</sup> and Se<sup>+</sup> ion implantation into SiO<sub>2</sub>

A. Markwitz<sup>a,b,\*</sup>, D.A. Carder<sup>a,b</sup>, T. Hopf<sup>a,b</sup>, J. Kennedy<sup>a,b</sup>, T.K. Chan<sup>d</sup>, A. Mücklich<sup>c</sup>, T. Osipowicz<sup>d</sup>

<sup>a</sup> GNS Science, 30 Gracefield Rd., Lower Hutt, New Zealand

<sup>b</sup> The MacDiarmid Institute for Advanced Materials and Nanotechnology, New Zealand

<sup>c</sup> Helmholtz-Zentrum Dresden-Rossendorf, Dresden, Germany

<sup>d</sup> Centre for Ion Beam Applications, Department of Physics, National University of Singapore, Singapore

### ARTICLE INFO

#### Article history:

Available online 29 July 2011

#### Keywords:

Ion implantation  
Nanoclusters  
Selenium  
Lead  
In-situ RBS  
In-situ ion implantation  
Fibre optics  
Solar cell technology

### ABSTRACT

First results obtained from electron beam annealed sequentially implanted Pb<sup>+</sup> (29 keV) and Se<sup>+</sup> (25 keV) ions into a SiO<sub>2</sub> matrix are presented. Key results from Rutherford backscattering spectrometry and transmission electron microscopy investigations are: (1) Pb and Se atoms are found to bond in the SiO<sub>2</sub> matrix during implantation, forming into nanoclusters even prior to the annealing step, (2) Pb and Se atoms are both present in the sample after annealing at high temperature ( $T = 760$  °C,  $t = 45$  min) and form into PbSe nanoclusters of varying sizes within the implanted region, and (3) the broader concentration profile of implanted Se creates a number of secondary features throughout the SiO<sub>2</sub> film, including voids and hollow shell Se nanoclusters. A sequential ion implantation approach has several advantages: selected areas of nanocrystals can be formed for integrated circuits, the technique is compatible with present silicon processing technology, and the nanocrystals are embedded in an inert matrix – making them highly durable. In addition, a higher concentration of nanocrystals is possible than with conventional glass melt techniques.

© 2011 Elsevier B.V. All rights reserved.

## 1. Introduction

First results obtained from sequentially implanting Pb<sup>+</sup> and Se<sup>+</sup> ions into a SiO<sub>2</sub> matrix at low-energy are presented. This system has been chosen due to the controversial role of surface states in PbSe nanocrystals. Due to the ionic character of the Pb–Se bond, the surface of bulk PbSe is free from surface states [1]. Theoretical models predict that the surface of PbSe nanocrystals is also free from states in the energy bandgap [2]. In the absence of passivation, it is theorised that Pb-rich nanocrystals have a large density of states in the bandgap [3]. Other recent studies have also experimentally demonstrated that the photo-properties are very sensitive to nanocrystal surface chemistry [4]. A widely tuneable system in nanocrystal form, PbSe is an ideal model system for this study [5]. A small effective mass for both electrons and holes allows the band gap to be modified in confined structures, from the bulk value of 0.28 eV to about 2.0 eV. This energy range spans from the visible to mid-infrared wavelengths, making PbSe nanocrystals a promising material for fiber-optic communication technology. PbSe nanocrystals have also generated great interest recently due to their potential use in solar cell technology.

\* Corresponding author at: GNS Science, 30 Gracefield Rd., Lower Hutt, New Zealand.

E-mail address: [a.markwitz@gns.cri.nz](mailto:a.markwitz@gns.cri.nz) (A. Markwitz).

## 2. Experimental

We have applied ion implantation and electron beam annealing to investigate the formation of PbSe nanocrystals in a SiO<sub>2</sub> host matrix. The ion implantations were performed with the recently developed ‘triple beam line’ implanter at GNS Science. Fig. 1 shows a simplified technical sketch of the newly developed ion implanter that is used for implanting ions from solid materials (e.g. metals) at low energy. The floor space requirements of the ion implanter are  $2 \times 1.5$  m.

The implanter has been developed to intersect with the RBS beam line of a 3 MV particle accelerator at 45°. A high current electron beam annealer has also been installed at the back of the RBS beamline. The three systems share the same sample chamber. Of importance is that a sample loaded into the chamber via a fast sample exchange chamber can be simultaneously implanted with metal ions, annealed at high temperature, and the profile of the implanted atoms can then be measured with RBS. The sample stage is freely rotatable so that individual sample treatments can be performed. The vacuum in the chamber reaches  $10^{-7}$  mbar, ensuring contamination-free materials processing and analysis. Some key details of the triple beam line ion implanter are: Penning sputter ion source with metal targets; terminal voltage 2–40 kV; electrostatic focusing and steering of the ion beam; 45° electromagnet with 40 mm pole gap and replaceable magnet chamber liners;

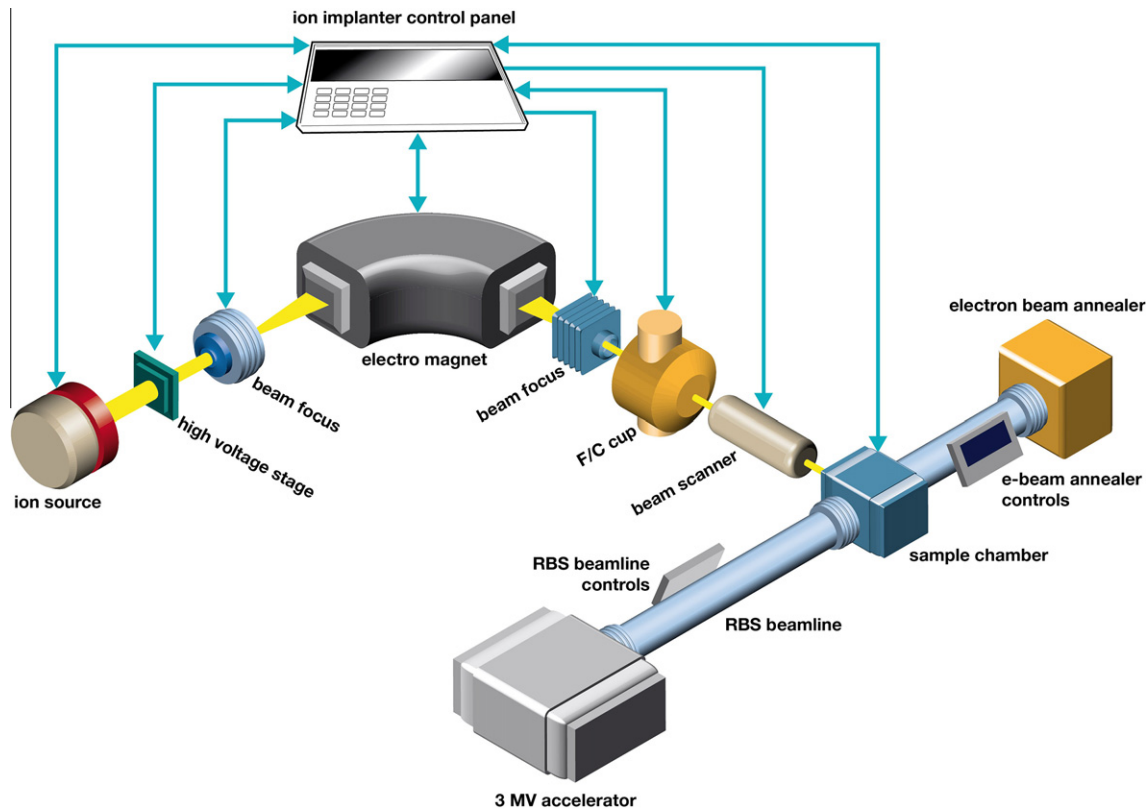


**Fig. 1.** Simplified conceptual design of the triple beam line implanter at GNS Science. Arrows indicate control and feedback systems. The sample chamber is connected to the RBS beam line and the high current electron beam annealer.

charge integrator controlled pneumatic Faraday cup in the beam-line to allow for semiautomatic ion implantation processes and electrostatic beam scanning. Areas of  $10 \times 10$  mm are laterally homogeneously implanted, as confirmed by RBS measurements.

Ion currents of less than  $10 \mu\text{A}$  were used in the experiments to reduce heating effects on the samples during implantation. It should be noted that the implanter was developed to fit in-between two existing RBS and proton microscopy beam lines. To perform ion beam analysis measurements during ion implantation uninterruptedly, electromagnetically shielded cages were developed for the ion source and their control units.

Dynamic TRIM was used to calculate the ion range, peak concentration and profile of Pb and Se ions [6]. This code considers variations in stopping power and sputtering yield during the Monte-Carlo calculations. It was found that 400 nm  $\text{SiO}_2$  layers on (1 0 0)Si are ideally implanted first with 29 keV  $\text{Pb}^+$  ions to the fluence of  $7 \times 10^{14} \text{ cm}^{-2}$ , and then with 25 keV  $\text{Se}^+$  ions implanted to  $9 \times 10^{14} \text{ cm}^{-2}$ , to create overlapping profiles at a depth of  $21 \pm 1$  nm with peak concentrations of up to 1 at.%.

The implanted samples were subsequently annealed with the computer controlled electron beam annealer at GNS Science [7]. A focussed 20 keV high current (typically 3–4 mA) electron beam was raster scanned over the implanted sample. The samples were annealed at  $760^\circ\text{C}$  for 45 min using temperature gradients of  $5^\circ\text{C s}^{-1}$  for the heating and cooling phases of the annealing cycle. At peak temperature, an accuracy of  $\pm 1^\circ\text{C}$  was obtained using a computer controlled feedback system that measures the surface temperature of the sample with a two-colour pyrometer. The electron current was monitored at the sample and at a Faraday cup positioned underneath the sample, and fine control of the electron beam current was achieved by varying the Wehnelt voltage of the electron gun. The annealing was performed under high vacuum of  $10^{-7}$  mbar.

RBS and PIXE techniques were used in the first step of analysis for QA/QC of the dual implanted Pb and Se samples. Elemental depth profiles were subsequently measured with high resolution elastic scattering at NUS, Singapore, using a 0.5 MeV  $^4\text{He}^+$  ion beam (beam to sample angle  $60^\circ$ ; sample to detector angle  $65^\circ$ ) [8]. An image-corrected FEI 80–300 TEM was used at the HZDR, Germany, to image cross-sectionally prepared TEM specimens.

### 3. Results

High resolution elastic scattering measurements were performed to investigate the depth profiles of the distribution of the implanted Pb and Se atoms before and after the annealing process. Fig. 2 shows a single distinct peak at 461.2 keV for the as-implanted sample indicating that both species, Pb and Se, have been successfully implanted into a similar depth. Simulations with RUMP show the distribution peaking at a depth of 22 nm (29.5 keV), considering the density of  $\text{SiO}_2$ . The FWHM of the distribution is calculated to extend from 12.8 nm (17.1 keV) to 44 nm (59 keV). In agreement with dynamic TRIM, Pb is not detected at the surface. The spectrum of the annealed sample shows three significant differences: (1) the distribution of the heavy elements is broadened, accompanied by a reduced concentration of heavy elements at the peak of the distribution; (2) Pb/Se is still not detected at the surface (depth resolution 1.1 nm) and (3) some Pb/Se atoms have diffused into the depth. These findings prompted the search for clustering at the surface, in the centre of the distribution and at the  $\text{SiO}_2/\text{Si}$  interface. Finding PbSe clusters is essential for any technological application. The specimens were cross sectionally prepared for high resolution TEM imaging using a well established preparation technique for crystalline silicon [9].

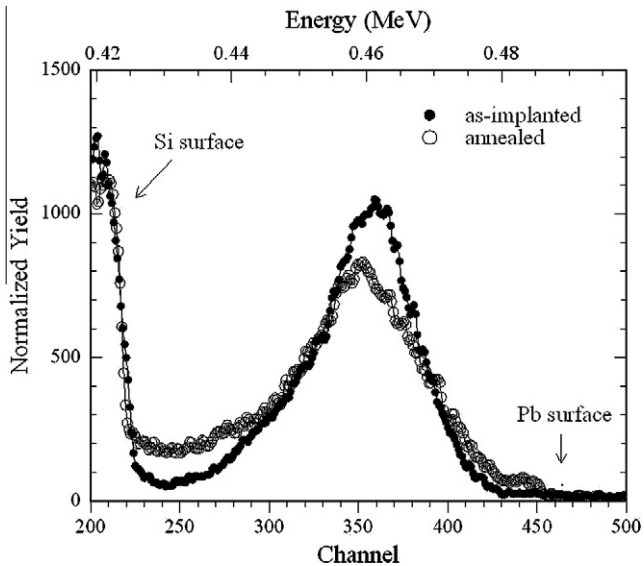


**Fig. 2.** High resolution elastic scattering measurements of  $\text{Pb}^+$  and  $\text{Se}^+$  ions implanted into  $\text{SiO}_2$  in the as-implanted and electron beam annealed state.

**Fig. 3** shows an overview image of the as-implanted sample in the near-surface region. The image was recorded with a magnification of  $245\times$  in a thin section of the sample, using an objective aperture to expose Pb and Se atoms. The image shows a band of heavy atoms at a depth of 22 nm. The width of the band is 23 nm, extending from 12.5 to 35 nm. The features in the centre of the band are bigger in size than at both ends of the distribution. EDX measurements confirmed the presence of both Pb and Se in this band, while neither Pb nor Se was detected at the surface and in the depth that stretches beyond the implantation depth. High resolution TEM images with magnification of  $300\times$  and  $620\times$  did not reveal any crystal lattices. The band was also imaged with HAADF, as shown in the inset in **Fig. 2**, to provide for better imaging of the size distribution. In this image, heavy atoms appear white in colour. The formation of a high density of small

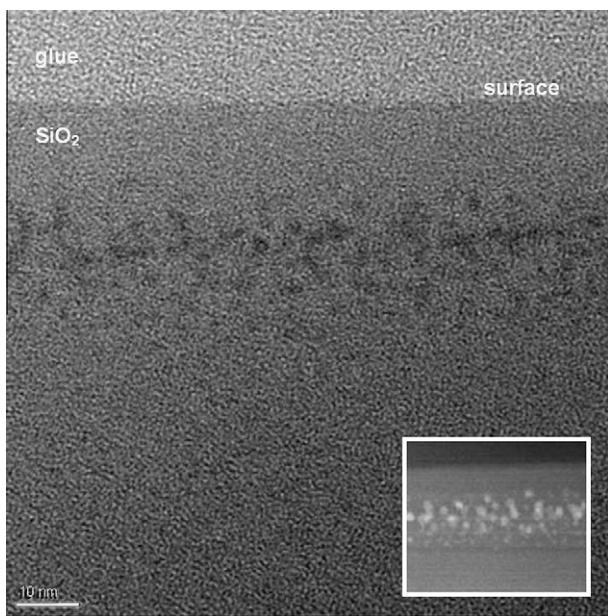


**Fig. 3.** Cross-sectional TEM image of the as-implanted  $\text{Pb}^+$  and  $\text{Se}^+$  ions in a  $\text{SiO}_2$  matrix. HAADF imaging in the inset shows that small nanoclusters begin to nucleate in the implanted region even before the annealing step.

nanoclusters within the implanted region can be observed, even prior to the annealing step. The nucleation of small nanoclusters in as-implanted samples has been previously detected for dual-element implantations into  $\text{SiO}_2$  [10] – including in similar systems like CdSe [11] – and it is likely that some degree of in situ sample heating due to the incident implantation current helps to trigger this nucleation process.

**Fig. 4** shows an overview TEM image of the sample after the high-temperature annealing step. The image was recorded in HAADF mode. Heavy element clusters appear white in the image, while holes in the thin section appear dark (black). As shown in the figure, the initial band of nanoclusters breaks up during annealing and a completely new configuration is formed. Pb and Se atoms are now spread across the 400 nm  $\text{SiO}_2$  layer in agreement with high resolution RBS measurements. Mainly small clusters (typical diameter 3–10 nm) appear close to the surface – but not at the surface – again in good agreement with high resolution RBS. These can be identified as PbSe nanoclusters with d-spacing of 0.305 (**Fig. 5**). This cluster band is most likely formed due to Ostwald ripening of the small PbSe nanoclusters that were observed in the as-implanted sample.

Near the centre of the  $\text{SiO}_2$  layer, far from the implanted region, occasionally large clusters appear. EDX shows that these have excess Se concentration. This trend continues for large clusters observed at the  $\text{SiO}_2/\text{Si}$  interface. Again, these clusters are mainly found to consist of Se. These results can be best understood as a consequence of the implantation profiles of Pb and Se. While the incident implantation energies were selected to create an overlapping band of Pb and Se centred at 22 nm depth, the much higher mass of the Pb atoms means that their distribution in the  $\text{SiO}_2$  will be significantly narrower. This will then lead to regions with excess Se concentration on either side of the central implantation band. Upon annealing this excess Se can form into nanoclusters, some of which are then able to diffuse deep into the substrate [12].

Interestingly, voids of a similar size to the clusters also appear in the near-surface region of the  $\text{SiO}_2$  after annealing. These kinds of voids are normally produced by heating nanoclusters above their boiling points, causing them to evaporate out of the sample [13]. While PbSe has a boiling point of over  $1000^\circ\text{C}$  – and should

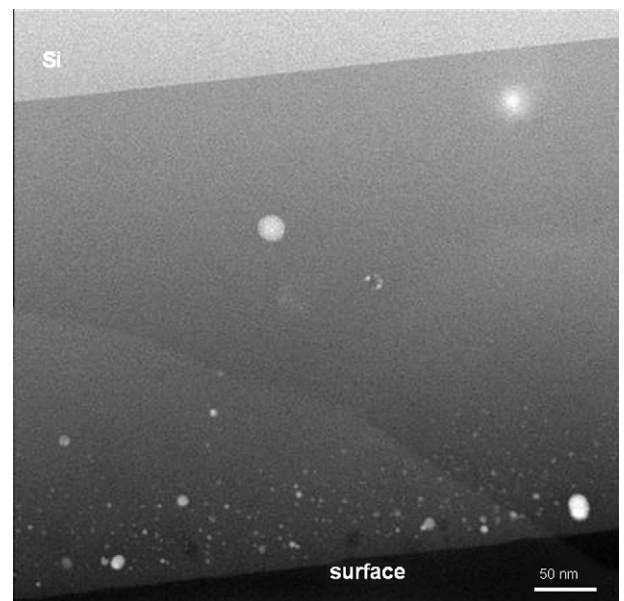


**Fig. 4.** TEM image (in HAADF mode) of the  $\text{SiO}_2$  sample after annealing at  $760^\circ\text{C}$  for 45 min. A number of different structures, including PbSe nanoclusters, voids, Se-only nanoclusters and hollow nanoclusters, can be observed within this sample.

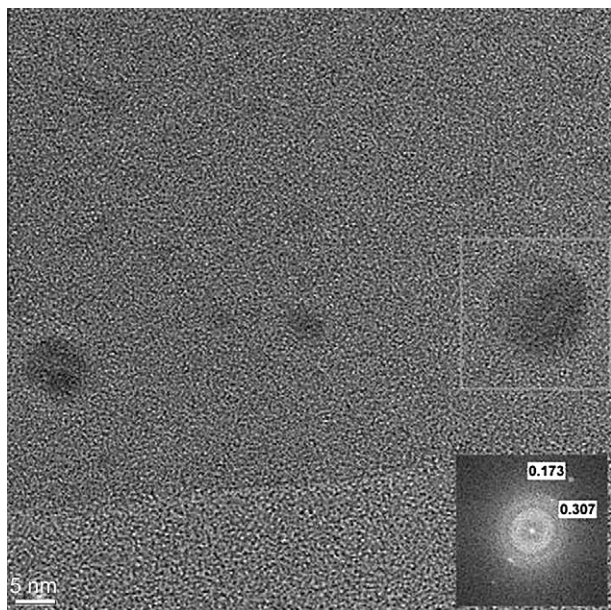


**Fig. 5.** TEM image of the near-surface region of the annealed  $\text{SiO}_2$  sample. The inset shows FFT analysis of a large cluster, revealing lattice spacings of 0.307 and 0.173.

thus be stable – the boiling point of Se is only 685 °C. Therefore, evaporation of the Se nanoclusters which form near the surface of the  $\text{SiO}_2$  due to the broader concentration profile of Se is to be expected after an annealing step at 760 °C. The hollow nanoclusters which are observed deeper in the sample after annealing are believed to have a similar origin: here, only partial evaporation of the Se nanoclusters may occur, and upon cooling this will lead to remnant Se wetting the edges of the void to form a hollow shell [13]. In-depth analysis with HAADF and EDX provides some evidence for this mechanism, confirming that the thin outer shell surrounding these clusters is indeed composed of Se.

#### 4. Summary

The key results of the investigations are: (1) Pb and Se atoms are found to bond in the  $\text{SiO}_2$  matrix during implantation, forming into

nanoclusters even prior to the annealing step (2) Pb and Se atoms are both present in the sample after annealing at high temperature and form into PbSe nanoclusters of varying sizes within the implanted region (3) the broader concentration profile of implanted Se creates a number of secondary features throughout the  $\text{SiO}_2$  film, including voids and hollow shell Se nanoclusters. A sequential ion implantation approach has several advantages: selected areas of nanocrystals can be formed for integrated circuits, the technique is compatible with present silicon processing technology, and the nanocrystals are embedded in an inert matrix – making them highly durable. In addition, a higher concentration of nanocrystals is possible than with conventional glass melt techniques.

#### Acknowledgements

The authors like to acknowledge the support from GNS Science Core Funding, FRST/MSI New Zealand and the Marsden fund from the Royal Society of New Zealand.

#### References

- [1] G. Allen, *Physical Review B* 43 (1991) 9594.
- [2] G. Allen, C. Delerue, *Physical Review B* 70 (2004) 245321.
- [3] A. Franceschetti, *Physical Review B* 78 (2008) 075418.
- [4] J.M. Luther, M. Law, Q. Song, C.L. Perkins, M.C. Beard, A.J. Nozik, *ACS Nano* 2 (2008) 271.
- [5] F.W. Wise, *Accounts of Chemical Research* 33 (2000) 773.
- [6] J.P. Biersack, S. Berg, C. Nender, *Nuclear Instruments and Methods in Physics Research B* 59 (1991) 21.
- [7] F. Fang, A. Markwitz, *Physica E: Low-dimensional Systems and Nanostructures* 41 (2009) 1853.
- [8] T. Osipowicz, H.L. Seng, T.K. Chan, B. Ho, *Nuclear Instruments and Methods in Physics Research B* 249 (2006) 15.
- [9] A. Markwitz, W. Matz, B. Schmidt, R. Grötzschel, *Surface and Interface Analysis* 26 (1998) 359.
- [10] E. Cattaruzza, *Nuclear Instruments and Methods in Physics Research B* 169 (2000) 141.
- [11] A. Ekimov, S. Gurevich, I. Kudriavtsev, O. Lublinskaya, A. Merkulov, A. Osinskii, M. Vatnik, M. Gandais, Y. Wang, *Journal of Crystal Growth* 151 (1998) 38.
- [12] R.E. de Lamaestre, F. Jomard, J. Majimel, H. Bernas, *Journal of Non-Crystalline Solids* 351 (2005) 3031.
- [13] A. Meldrum, S. Honda, C.W. White, R.A. Zuhr, L.A. Boatner, *Journal of Materials Research* 16 (2001) 2670.